Green Analytical Chemistry 16 (2026) 100327

Contents lists available at ScienceDirect

Green Analytical Chemistry

journal homepage: www.elsevier.com/locate/greeac

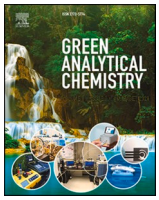

A sustainable analytical workflow for microplastic detection and typification via NIR-HSI: Validation through sea salt analysis

Miriam Medina-García [a], Jose Manuel Amigo [b,c,*], Giulia Gorla [b], Enmanuel Cruz-Muñoz [d], Davide Ballabio [d,*], Miguel A. Martínez-Domingo [e], Eva M. Valero [e], Ana M. Jiménez-Carvelo [a,*]

[a] Department of Analytical Chemistry, Faculty of Sciences, University of Granada, Av. Fuentenueva s.n., 18071 Granada, Spain
[b] Department of Analytical Chemistry, Faculty of Science and Technology, University of the Basque Country UPV/EHU, Sarriena s/n, Leioa, Basque Country 48940, Spain
[c] IKERBASQUE, Basque Foundation for Science, 48011, Bilbao, Spain
[d] Department of Earth and Environmental Sciences, University of Milano-Bicocca, P.zza della Scienza 1, Milano 20126, Italy
[e] Department of Optics, Faculty of Sciences, University of Granada, Av. Fuentenueva s.n., 18071 Granada, Spain

ARTICLE INFO

Keywords:
Pollution monitoring
Microplastics
Green analytical method
Imaging
Machine learning
NIR

ABSTRACT

This work presents a sustainable analytical workflow for the detection and typification of microplastics (MPs) in environmental matrices using Near Infrared Hyperspectral Imaging (NIR-HSI) combined with chemometrics. The proposed methodology enables rapid, non-destructive, and solvent-free analysis, aligning with green analytical principles. A hierarchical classification strategy based on Partial Least Squares Discriminant Analysis (PLS-DA) was developed to discriminate between salt and MP spectra and subsequently to typify the polymeric nature of the detected MPs.

Four of the most prevalent polymers in the Mediterranean Sea (polyethylene (PE), polyethylene terephthalate (PET), polystyrene (PS), and polyvinyl chloride (PVC)) were selected as reference standards. The workflow was first optimised and validated using reference and simulated salts and then applied to real sea salt samples collected from Mediterranean coastal saltworks and commercial grocery salts. The results demonstrated excellent classification performance, with 100 % sensitivity, specificity, and precision in both validation stages. Among the analysed samples, MP contamination was confirmed in 3 coastal and 2 commercial salts, with PET and PE being the dominant polymers. These findings highlight sea salt as a valuable proxy for marine MP contamination and as a potential route of human exposure. Overall, this study introduces a green, efficient, and reproducible analytical approach for MPs detection and typification, providing a foundation for future large-scale environmental monitoring and risk assessment initiatives.

1. Introduction

According to the *United Nations Environment Programme (UNEP)*, microplastics (MPs) are defined as plastic fragments which size ranges from 5 mm to 1 μm [1]. They can be broadly categorised into two groups based on their origin being primary or secondary.

Primary MPs are intentionally manufactured in microscopic dimensions, ranging from millimetres to micrometres, for their incorporation into domestic and personal care products such as defoliants, toothpaste, detergents, and certain cosmetic formulations. This category also includes pre-production plastic pellets, commonly known as *nurdles*, which serves as a raw material in the plastic industry. These pellets may be unintentionally released into the environment during transport, handling or storage, representing a significant source of contamination [2,3].

In contrast, secondary MPs, which are by far the most prevalent type found in natural environments, originate from the fragmentation of larger plastics items. Typical sources include products such as plastic bags, bottles, fishing nets and packaging materials. Their fragmentation is driven by various abiotic and biotic factors, including ultraviolet (UV) radiation, mechanical abrasion and microbial activity. The resulting plastic fragments exhibit high environmental persistence, accumulating

* Corresponding authors.
E-mail addresses: josemanuel.amigo@ehu.eus (J.M. Amigo), davide.ballabio@unimib.it (D. Ballabio), amariajc@ugr.es (A.M. Jiménez-Carvelo).

https://doi.org/10.1016/j.greeac.2026.100327
Received 31 October 2025; Received in revised form 14 January 2026; Accepted 2 February 2026
Available online 2 February 2026

in aquatic systems (including oceans, rivers, and lakes), soils and the atmosphere [4].

MPs pose a wide range of adverse effects on biological health, which can be distinguished into physical and chemical. Physical effects include entanglement, ingestion and their accumulation within organisms, as previously highlighted. In the particular case of marine ecosystems, MPs are readily incorporated into organisms through direct ingestion or filtration. Upon ingestion, these particles may trigger inflammatory responses by adhering to or penetrating intestinal walls, potentially impairing normal physiological functions. The consequences extend further across trophic levels: small invertebrates that ingest MPs become vectors of contamination for larger predators, while filter-feeding megafauna such as whales are exposed both through the consumption of contaminated prey and through the filtration of wide volumes of seawater. In this manner, MPs enter and propagate through marine food webs, undergoing bioaccumulation and biomagnification across multiple trophic levels, ultimately reaching humans [5]. Emerging evidence highlights the extensive impact of MPs in living organisms, with studies confirming their presence in animals as well as in humans bloodstream, their stomach and brain [6–9].

Beyond their physical effects, MPs also induce a range of chemical impacts. These materials can absorb environmental pollutants such as pesticides and chlorinated biphenyl, which cause chronic effects, including endocrine disruption, mutagenicity and even cancer [1]. Upon ingestion by birds, mammals and fish, MPs can act as vectors for these absorbed pollutants, allowing their transfer through food webs. An additional concern arises from the additives incorporated into plastics to confer properties such as durability, UV resistance, and flexibility, which can also cause adverse effects. In response to these concerns, non-governmental organizations (NOGs) have initiated a range of actions aimed at raising awareness, promoting education and influencing policy through targeted lobbying efforts. These initiatives include public education campaigns, coastal clean-up activities, and ocean expeditions to document and remove litter. Given that the current technology is insufficient to eliminate MPs from marine environments, additional efforts have focused on the development of methodologies to monitor, mitigate and prevent their occurrence [10,11].

Environmental studies on monitoring MPs impact have primarily focused on soil, water and the atmosphere analysis. MPs tend to accumulate on the soil surface through multiple pathways, including direct deposition from nearby sources, runoff from contaminated waters and atmospheric deposition. Soil samples are typically subjected to complex pre-treatment procedures before the analysis, often involving digestions to remove organic matter and sieving through meshes of varying pore sizes to isolate these pollutants. Marine environments have also been studied applying two main approaches: collecting MPs floating at the water surface with trawl nets or directly sampling water aliquots, which are subsequently subjected to digestion and filtration to recover MPs [12]. Atmospheric samples are usually obtained via passive deposition collectors or active pumped samplers, and they are subjected to a digestion process and particle separation based on density [13]. Beyond these conventional matrices, alternative indicators have been employed, such as marine organisms and sea salt, both of which serve as indicators of MPs pollution in seawater [14,15].

Sea salt represents a particularly interesting matrix for the study of MPs pollution in seawater. Solar saltworks act as large-scale natural pre-concentrators of the pollutants present in seawater, due to the sequential processes of evaporation and crystallisation that occur during salt extraction. This natural pre-concentration mechanism provides a unique opportunity to investigate the occurrence and composition of MPs in seawaters, using sea salt both as a proxy for environmental contamination and as a direct route of human exposure through dietary intake.

Although sampling and pre-treatment protocols differ among matrices, all generally involve chemical digestion and particle separation, underscoring that direct analysis of environmental samples is rarely feasible.

The most employed analytical methods for the detection and typification of MPs in environmental matrices include visual inspection, Fourier-transform infrared spectroscopy (FTIR), Raman spectroscopy, scanning electron microscopy (SEM) and pyrolysis coupled with gas chromatography–mass spectrometry (Py-GC/MS) [16,17]. Visual inspection, although it is simple, rapid and can provide information about the morphology and colours, it is inherently limited by subjectivity, low visual capacity of small samples, and the inability to reliably differentiate plastics from non-plastic particles of similar appearance. The remaining techniques, while more accurate, require laborious sample pre-treatments, often involve the use of chemical solvents, and are characterised by high operational costs and long analysis times. In response to these challenges, new methodologies have been developed based on imaging technologies such as Near Infrared Hyperspectral Imaging (NIR-HSI).

NIR-HSI combines imaging techniques with spectroscopy, enabling the simultaneous acquisition of spatial and spectral information across a broad wavelength range, and resulting in an image of a material that is indirectly related to its chemical properties. This technique is non-destructive/non-invasive, rapid, and covers the spectral region corresponding to polymer fingerprint bands, as C—H, N—H, C—C, and C—O absorption bands (1100 to 2500 nm) [18]. NIR-HSI generates a large volume of data, which are usually analysed by means of chemometric tools, such as Principal Component Analysis (PCA), Soft Independent Modelling of Class Analogy (SIMCA), Support Vector Machine (SVM) or Partial Least Square Discriminant Analysis (PLS-DA). NIR-HSI has proven to be a powerful technique for reliable identification of these pollutants across a variety of environmental matrices [19,20].

These approaches align with international initiatives that not only encourage the development of innovative strategies for monitoring MPs contamination but also advocate for greener and more sustainable analytical methodologies. Despite the demonstrated potential of NIR-HSI, one of the main limitations identified in the literature is its applicability to real environmental samples. Nyakuchena et al. highlight the capability of combining HSI with advanced data analysis techniques, such as deep learning, to classify up to six isolated MPs types [21]. Palmiery et al. applied a hierarchical analysis methodology to successfully identify microplastics extracted from real Mediterranean seawater using trawl nets [22]. While these studies clearly demonstrate the potential of NIR-HSI for microplastic classification, a key challenge highlighted by Goyetche et al. [19] remains unresolved: the direct application of these methodologies to real-world scenarios with complex matrices.

Building upon previous work that combined NIR-HSI and chemometric tools to monitor MPs in Mediterranean seawater, where real sea salt from coastal saltworks was successfully employed as an indicator of contamination [23], the present study advances the field by enabling not only the detection of MPs but also their typification, i.e., the identification of the type of polymer each MPs is compound. The main focus of this study was to develop a green analytical workflow based on NIR-HSI that does not require sample pre-treatment involving solvents or chemical reagents. Beyond method development, this work demonstrates the practical application of this approach to real environmental samples, showing that microplastics can be detected and identified even when embedded within complex matrices. In addition, the method improves spatial resolution and extends the spectral range from 900–1700 nm (spectral range of the camera used in the previous study [23]) to 2505 nm. The extension is particularly relevant because it expands the coverage of the short-wave infrared (SWIR) region, which contains many of the most informative absorption features of polymeric materials.

For the analysis of the resulting spectral data, PCA was applied as an unsupervised exploratory method to examine the natural grouping of spectra extracted from hyperspectral images. In addition, PLS-DA was employed to develop a hierarchical classification model capable of detecting and typifying MPs.

Table 1
Overview of salt samples collected for this study.

Salt sample	No of samples
Blank salt	106
Simulated MPs free salt	1
Sea salt	54
Grocery salt	6

One of the major advantages of employing NIR-HSI over conventional single-point spectrophotometry lies in its ability to capture spatially resolved chemical information. This capability is particularly relevant for microplastic analysis, as MPs can be heterogeneously distributed throughout the sample. A point-based measurement could easily miss localised particles, leading to incomplete or biased results. In contrast, NIR-HSI provides a comprehensive mapping of the entire sample surface, ensuring that the acquired data are representative not only of the bulk composition but also of its spatial variability.

2. Materials and methods

The methodology developed in this work required the recompilation of two types of sample banks: (i) reference set of MPs standards and (ii) salts. A detailed account of the collection and selection processes for the samples included in both banks is provided below.

2.1. MPs standards

The MPs standards bank was compiled by selecting the four polymers with higher prevalence in the Mediterranean Sea, as reported in the literature: polyethylene (PE), polyethylene terephthalate (PET), polystyrene (PS) and polyvinyl chloride (PVC). It should be noted that these polymers were recognised as promising indicators to monitor MPs in the environment [24–26]. For that, chemically pure standards of these polymers were purchased from a recognised supplier (Sigma-Aldrich, Darmstadt, Germany).

2.2. Salt samples

To compile the salt bank, four types of salts were selected:

i. **Blank salts:** they were collected from inland saltworks, specifically from *La Malahá* (Granada, Spain), and were considered unpolluted salts as they had no contact with seawater.
ii. **MPs-free simulated sea salt reference:** due to the blank salt composition not being the same as sea salt, artificial unpolluted salt was prepared in the laboratory to simulate the chemical composition of salt extracted from Mediterranean coastal saltworks. The salt was formulated using the following compounds: NaCl (62.9 g/100 g), $MgCl_2$ (11.4 g/100 g), $CaCl_2$ (2.1 g/100 g), KCl (2.1 g/100 g), Na_2SO_4 (17.7 g/100 g), $MgSO_4$ (2.9 g/100 g), and $CaSO_4$ (1.2 g/100 g). The proportions were adjusted based on literature and correspond to the concentrations of inorganic salts present in the Mediterranean Sea [27].
iii. **Coastal sea salts:** real salts obtained from solar saltworks located along the Andalusian Mediterranean coast, particularly from *Cabo de Gata* (Almeria, Spain), were collected. These salts were considered potentially contaminated due to their direct contact with Mediterranean seawater in which MPs have been detected and served as indicators of the presence of MPs in Mediterranean seawater. MPs may be dispersed within these salts due to the natural pre-concentration process occurring in solar saltworks during the extraction of sea salt.
iv. **Grocery sea salts:** these samples were included as exposure pathway indicators, representing salts that may be consumed directly by humans. They were purchased from local supermarkets in Spain. They are sourced from various brands and regions across the country. In addition, one sample of Himalaya salt was also collected.

Following the collection of the samples, all salt samples were subjected to mill in a laboratory milling device (IKA, A10 basic, Staufen, Germany) for 15 s to reduce and homogenise particle size. Table 1 summarises the types and number of salt samples:

It should be noted that the number of samples varied according to their nature and representativeness requirements. A larger number of blank salt and coastal sea salt samples were collected because they were taken from different crystallisers and evaporation ponds and from different production seasons, in order to obtain a representative sample bank of the entire salt production area. For the grocery sea salts, several samples from different commercial brands and origins were included to reflect the variability of the products available on the market. In contrast, only one sample of MPs-free simulated sea salt reference and MPs standards were collected, as these represent pure reference materials, and a single sample was sufficient to provide representative spectral information about them.

All samples were subsequently placed in glass Petri dishes until the surface was completely covered, preparing the samples for further analysis using NIR-HSI.

2.3. NIR-HSI measurements and data processing

For this study NIR-HSI images were captured using the SWIR SPECIM hyperspectral camera (SPECIM, Oulu, Finland) in reflectance mode. The spectral range of this instrument spans in the range 996 - 2505 nm, split into 272 bands with a spectral resolution of 5,5 nm. Each scan line consisted of 384 spatial pixels with a real sampling pixel size of 43 × 190 μm with a total of 1470 lines collected per image. The exposure time was 4.5 ms per line, yielding a frame rate of 120 Hz. No spectral binning was applied. The capturing distance was established at 25 cm, corresponding to the minimum achievable by the camera, in order to reach the highest spatial resolution. The scanning speed was set at 5.00 mm/s.

NIR-HSI images were captured in batches of two samples: A quality control (QC) sample to verify that analysis conditions remain constant through the capturing process, and one of the samples under study. A dark reference was obtained automatically by the system through shutter closure, while a Spectralon standard was used as a white reference and acquired in each measurement. Each image was corrected using the measures of both reference standards. Further processing was conducted using MATLAB R2022a software (MathWorks Inc., Natick, MA, USA). The software was used for the definition of ROI and for the pre-processing and data analysis steps.

ROI selection was performed as follows: first, the central coordinates of each Petri dish were identified and defined, and then only the pixels within its interior were selected. A fixed number of 331,000 pixels (spectra) was extracted per Petri dish (per sample). This number was selected to cover the entire area of the Petri dish, excluding the borders and ensuring that the same number of pixels is selected in all cases. All extracted spectra were then vertically concatenated, resulting in a data matrix of 331,000 × 272 elements for each sample.

In the case of batch-to-batch QC samples, the average spectrum of the data matrix was calculated, and then, the nearness index (NEAR) was applied to study the similarity between each pair of average spectra [28]. The NEAR index evaluates the similarity between two spectral vectors based on the calculation of the Euclidean distance between them. Eq. (1) defines how to calculate the NEAR index for two vectors, Y_A and Y_B, where d^N is the normalised distance and d_{max} is the maximum distance between points. This index is normalised between 0–1. A value closed to the unit indicates that the analysis conditions remained constant. In this case, the conformity limit was established at higher than 0.95.

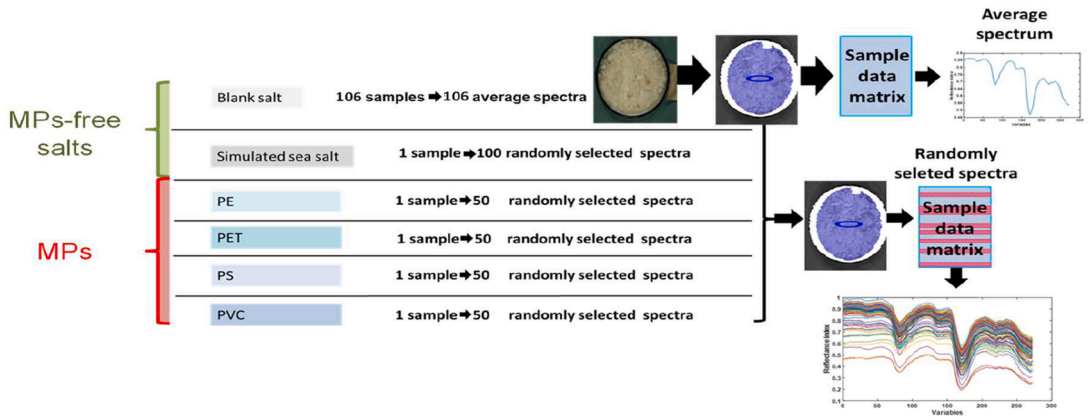

Fig. 1. Schematic overview of the approach adopted to build a representative working dataset.

$$\mathrm{NEAR}(\mathbf{Y_A},\ \mathbf{Y_B}) = 1 - \mathrm{d}^{\mathrm{N}}\ (\mathbf{Y_A},\ \mathbf{Y_B}) = 1 - \frac{\mathrm{d}\ (\mathbf{Y_A},\ \mathbf{Y_B})}{\mathrm{d}_{\max}\ (\mathbf{Y_A},\ \mathbf{Y_B})}$$
$$= 1 - \sqrt{\frac{\sum (y_{Ai} - y_{Bi})^2}{\sum (y_{Ai} + y_{Bi})^2}} \quad (1)$$

Once it was verified that the analysis conditions had remained constant throughout the measurement process, the next step was to define the working dataset.

As noted above, the study considered five categories of samples: (i) MPs standards, (ii) blank salts, (iii) MPs-free simulated sea salt reference (hereafter referred to as *simulated salts*), (iv) coastal sea salts and (v) grocery sea salts. For the working dataset definition, only the first three categories (i, ii, iii) were included. Coastal and grocery sea salts were excluded from this stage and reserved exclusively for the final prediction phase.

Considering this, the working dataset was defined with two objectives in mind: (i) develop a classification model capable of discriminating between MPs-free salt and MPs spectra; (ii) identify the specific polymer type that generates each spectrum classified as MPs. To achieve this, the dataset was balanced to include approximately equal number of MPs-free salt and MPs spectra, and also equal number of spectra for each polymer type. Considering the imbalance in the number of samples of each sample type, the approach outlined in Fig. 1 was followed to build the dataset.

In the case of blank salt, 106 samples were collected. From each one, the average spectrum was calculated from its corresponding data matrix and included in the working dataset, adding up to a total of 106 spectra. For the remaining types, of which only one sample was available, a subset of spectra was randomly selected: 100 spectra in the case of simulated salt and 50 spectra for each polymer type (PE, PET, PS and PVC). They were also included in the working dataset. In this way, the final dataset consisted of 206 spectra from MPs-free salts and 200 spectra of MPs, resulting in a data matrix of 406 × 272 elements.

2.4. Comparison of analytical information between hyperspectral cameras

As explained in the introduction, this work builds on a previous study where the developed methodology based on NIR-HSI showed high effectiveness for the detection of MPs in sea salts. In the present study, the scope is expanded towards MPs typification. In this context, a comparative evaluation of two hyperspectral systems was undertaken in order to assess the influence of sensor type and spectral range on the information content of the acquired signals. The first system (Camera 1) operates in the 900–1700 nm spectral range using an InGaAs sensor, while second system (Camera 2), used in the present study, covers the 996–2505 nm range with an MCT sensor. The commercial models used were the Resonon Pika NIR+ (Resonon, Inc, Canada) and the SPECIM SWIR (SPECIM, Oulu, Finland), respectly.

Shannon's entropy was employed as a theoretical measure to quantify the information of the spectral data provided by each camera. This comparison aimed to determine the instrumental configuration that offers the most informative basis for subsequent data modelling. Particularly, Shannon's entropy can be defined as a measure of the average information content in a signal and can be expressed mathematically as the Eq. (2) [29]:

$$H_S = -\sum_i (P_i \cdot \log_{10} P_i \quad (2)$$

where H_s represents the information entropy and p_i the probability associated with each data point of the signal. The probabilities were calculated as the ratio between each intensity value and the total sum of intensities, which is mathematically equivalent to applying total sum normalization to the spectrum. Within this framework, higher values of H_s indicate lower information content in the signal. This metric can be normalised between 0–1 units, resulting in Shannon's information index (I_s) (Eq. (3)):

$$I_S = 1 - \frac{H_s}{H_s(\max)} \quad (3)$$

where H_s(max) represents the maximum entropy achievable for the spectral signal. This maximum corresponds to a perfectly uniform distribution of intensity values across all wavelengths and is calculated as $\log_{10}(n)$, with n being the number of spectral variables (wavelengths) in the signal. It should be noted that, although a base-10 logarithm is used here, any other logarithmic base could be applied without affecting the relative ratio to H_s(max).

One hyperspectral image per camera was acquired for each type of MPs standard (PE, PET, PS and PVC). The region of interest (ROI) was defined for each image, and the corresponding average spectrum was calculated. Then, they were evaluated with Shannon's index. The resulting values were compared to assess which instrument provided MPs standard spectra with higher information content, thereby informing the choice of the most suitable hyperspectral system for MPs typification.

2.5. Hierarchical classification modelling

Prior to the data analysis step, spectra were pre-processed using standard normal variate (SNV) and mean centring. As an initial step, PCA was applied as an unsupervised exploratory method in order to evaluate whether the dataset exhibited grouping patterns.

After the exploratory analysis, a hierarchical classification strategy was applied. The hierarchical classification strategy comprised two

Table 2
Strategy and distribution of spectra between training and external validation sets for the development of binary and multiclass models.

Model	Samples involved	No of spectra (training set)	Total Spectra per class	No of spectra (validation set)	Total Spectra per class
Binary	Blank salt	74	144	32	62
	Simulated salt	70		30	
	PE	35	140	15	60
	PET	35		15	
	PS	35		15	
	PVC	35		15	
Multiclass	PE	35	35	15	15
	PET	35	35	15	15
	PS	35	35	15	15
	PVC	35	35	15	15

sequential models: (i) a binary model (MPs vs. MPs-free salt), designed to discriminate between spectra originating from MPs-free salts and those associated with MPs, addressing the primary analytical challenge of detecting microplastics within a dominant environmental matrix; and (ii) a multiclass model (PE vs. PET vs. PS vs. PVC), built exclusively using MPs spectra in order to differentiate among the four polymer types once the presence of MPs had been established. In this way, a two-level framework was intentionally implemented to reflect a realistic analytical workflow, in which the first stage focuses on the detection of MPs in a real environmental matrix, while the second stage enables polymer identification only for samples previously classified as MPs. This hierarchical approach allows the influence of the salt matrix to be considered during the detection step, without compromising polymer differentiation, thereby facilitating the application of the methodology to real sea salt samples (see Figure S1 for further details on the hierarchical model workflow).

Both models were developed using PLS-DA method. PLS-DA is essentially based on the PLS2 algorithm that searches for latent variables with a maximum covariance with the Y-block, which defines sample labels with a dummy matrix [30]. For each sample, PLS-DA returns the predictions with values in-between 0 and 1: a value closer to zero indicates that the sample does not belong to the class, while a value closer to 1 the opposite. In order to define classification labels, class thresholds can be defined, and each sample can be assigned to the class if its predicted value is higher than the defined threshold [31].

To build models, working dataset was split into training (70 %) and validation (30 %) subsets within each material type (see Table 2). Splitting was carried out by means of the Kennard-Stone algorithm [32]. Both subsets were pre-processed applying standard normal variate (SNV) and mean centring. Particularly, validation subset was mean centred with the mean of training subset. This procedure ensured that validation samples did not contribute to the pre-process, thereby simulating a real prediction scenario.

Binary model was trained with samples labelled as MPs-free salts and MPs, while multiclass model was trained with samples labelled on the basis of four classes, corresponding to the polymer types under study: PE, PET, PS, PVC. This model was calculated using the training samples previously selected for binary Model A and labelled as MPS. For both binary and multiclass models Model A and Model B, cross validation with 5 splits was used for determining the optimal number of latent variables within each PLS-DA model. Models were externally validated using the validation samples.

It is important to highlight a key aspect of the working dataset building. As previously mentioned, for materials represented by only one sample (simulated salt, PE, PET, PS and PVC), random spectra were extracted from their respective ROIs. To ensure that the random selection of spectra did not affect the representativeness of the sample and also compromise the classification performance, the hierarchical model

Table 3
Values of Shannon's information indices (Is) calculated from the average spectrum of PE, PET, PS, and PVC measured using hyperspectral cameras 1 and 2.

Polymer	I_S (Camera 1) 900 – 1700 nm	I_S (Camera 2) 996 – 2505 nm
PE	0.023	0.029
PET	0.007	0.017
PS	0.025	0.090
PVC	0.023	0.017

modelling process was repeated 1000 times. In each iteration, new subsets of spectra were randomly sampled, thereby both models were trained and then validated with 1000 different working datasets, each consisting of 406 spectra. Robustness was assessed by calculating specificity, sensitivity and precision quality metrics of each iteration.

Data analysis was performed using the PLS_Toolbox (Eigenvector Research, WA, USA) in the Matlab environment. The development of the hierarchical classification models was performed with ad-hoc MATLAB functions, with PLS-DA models developed using the MATLAB Classification Toolbox [33,34].

2.6. MPs detection and typification in salts

Once the hierarchical model has been trained, validated, and its performance assessed, the final prediction stage was performed. In this step, coastal sea salts and grocery sea salts were analysed. Each sample was processed individually, considering all spectra within its ROI (a total of 331,000 spectra per sample).

In the first stage, binary model was applied to discriminate between spectra from MPs-free salts and those from MPs. Then, multiclass model was applied exclusively to the spectra identified as MPs in order to determine the polymer type (PE, PET, PS or PVC). After classification, the relative abundance of each class was estimated for every sample. This was calculated at both levels of the hierarchical framework (A and B) using the Eq. (4):

$$\mathrm{RA}\ (\%) = \frac{P_X}{P_T} \cdot 100 \tag{4}$$

Where RA (%) is the relative abundance of class X in percentage, P_X is the number of pixels classified as class X, and PT is the total number of pixels within the ROI (in this case, 331,000 pixels). Additionally, representative spectra classified as MPs-free salt and as specific type of polymer were plotted to visually assess whether real spectral differences could be observed.

3. Results and discussion

3.1. Selection of the most informative hyperspectral signal to modelling

The most informative hyperspectral signal was selected by comparing the reflectance average spectra of each polymer type under study (PE, PET, PS and PVC) measured by both Camera 1 and Camera 2. No signal pre-processing was applied in this stage, beyond the calibration to obtain reflectance data from raw captures. It should be noted that only polymer spectral signals were compared, as the main objective of this study is to develop a method capable of discriminating among them.

In order to evaluate the information content of the spectra obtained by each hyperspectral camera, Shannon's information index (I_S) was calculated for each average spectrum (Eqs. (2) and 3). The results are presented in Table 3. In all cases, the information index values from spectra obtained by the Camera 2 were more informative, except for PVC. This finding is coherent with the literature, where the spectral fingerprints of the four polymers have been identified in the wavelength range 1100 to 2500 nm.

These results indicate that the hyperspectral signals acquired with Camera 2 are more suitable for the application of unsupervised methods,

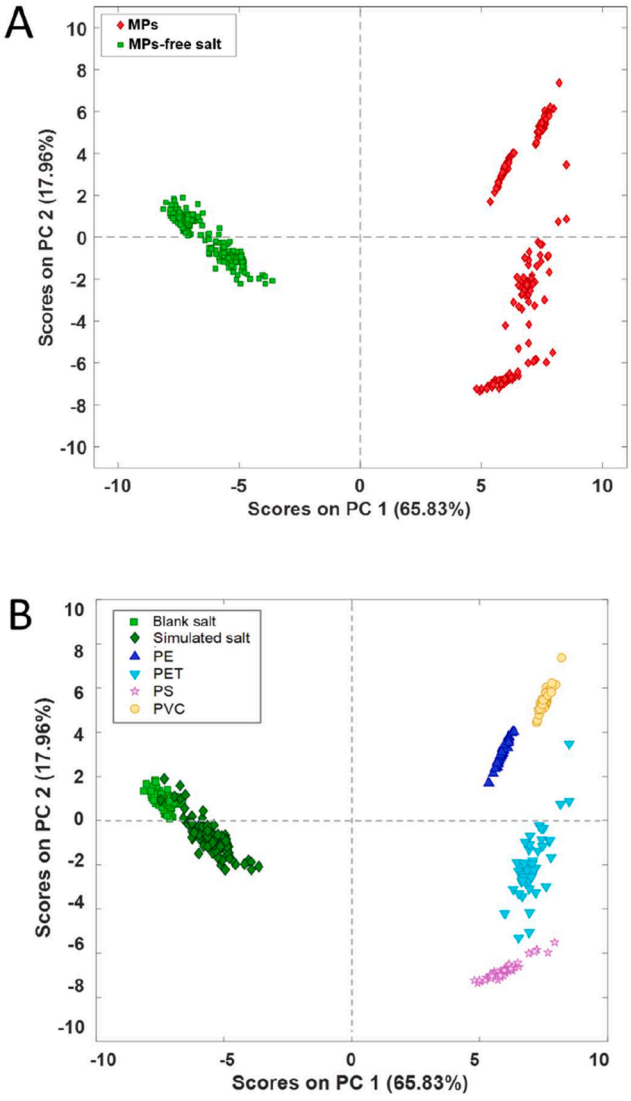

Fig. 2. PC1 versus PC2 scores plot representing spectra extracted from hyperespectral images captured from salt and MPs matrixes, labelled as: (A) MPs-free salt and MPs; (B) blank salt, simulated salt, PE, PET, PS and PVC.

as well as, supervised methods for classification tasks.

3.2. Exploratory analysis

In order to identify behavioural patterns among samples, PCA was applied to the pre-processed dataset, constituted by 406 spectra represented by 272 variables (i.e., wavelengths). PC1 and PC2 accounted for 65.83 % and 19.96 % of the total variance (87.79 %). The scores plot of PC1 and PC2 represents the most significant variability between samples. Fig. 2A shows PC1 vs PC2 scores plot considering two broad types of spectra: spectra extracted from MPs-free salts (green squares) and from MPs (red rhombuses). A clear separation is observed along the PC1. MPs-free salt spectra tend to exhibit negative scores in this component, while MPs spectra show positive values. This indicates that the major source of variance captured by PC1 is directly related to the distinction between salt and MPs matrices, highlighting the feasibility of building a classification model to separate both.

Fig. 2B represents the same scores plot, but here the spectra are labelled according to each individual sample type (blank salt, simulated salt, PE, PET, PS and PVC). It reveals a clear, close grouping between blank salts and simulated salts, albeit slightly shifted along PC1 and PC2, suggesting subtle compositional differences. It makes sense because the salts sampled from inland saltworks have compositional characteristics that are expected to differ from those of the simulated salt, which was artificially prepared to mimic coastal salt from the Mediterranean Sea. However, the most important observation concerns the distribution of the spectra extracted from the different types of polymers. Notably, distinct clustering patterns were observed among them, indicating that each polymer type could be clearly distinguished. It demonstrates the potential of multivariate analysis to discriminate not only between MPs-free salts and MPs contamination but also among MPs types, laying the groundwork for a hierarchical classification model.

Following the inspection of the PCA score plots, the corresponding loading bi-plot of PC1 and PC2 (Fig. 3, top) was examined to explore the spectral regions contributing to the main sources of variance in the dataset. In the same figure, the average spectra of each sample type (MPs free salts and MPs) are also presented as a visual spectral reference to support the interpretation of the loading patterns.

PCA loadings describe how wavelengths contribute to the variance captured by each principal component. Accordingly, the loading profiles were used to qualitatively relate spectral regions to the sample distribution observed in the score plots. As discussed above, PC1 captures the dominant variability associated with differences between MPs-free salt samples and MPs. Positive PC1 loadings therefore indicate spectral regions that are more strongly associated with samples exhibiting MP-related spectral features. These regions are mainly located within the 1400–1700 nm (variables 60–125) and 1900–2300 nm (variables 160–225) intervals.

Inspection of the average spectra within these wavelength ranges confirms that the observed separation is supported by clear spectral differences (see purple border of Fig. 3). In both intervals, simulated salt and blank salt samples exhibit a pronounced reflectance minimum, whereas all studied polymer types display broader reflectance features with an opposite spectral trend, resulting in a marked contrast between MP-free salts and MP spectra. A similar behavior is observed in the second interval (1900–2300 nm), further supporting the relevance of these regions for distinguishing microplastics from the salt matrix.

A more detailed inspection of polymer-related spectral patterns suggests that PS and PVC samples, which exhibit positive scores in both PC1 and PC2, show higher variability predominantly within the 1400–1700 nm region, whereas PE and PET samples present more pronounced contributions within the 1900–2300 nm interval. Although these trends arise from an unsupervised analysis, they are consistent with known NIR absorption features of the investigated polymers. These observations further highlight the relevance of employing a hyperspectral system covering the full NIR range to enable reliable MPs detection and typification.

3.3. MPs-free salts vs microplastics

PLS-DA binary model was developed, defining two input classes (2iC): labelled as 'MPs-free salt' and 'MPs'. MPs-free salt class comprised spectra from blank salts and simulated salts, while MPs class was defined by the spectra extracted from MPs standards under study. The model was built selecting 1 LVs, which explained 64.39 % and 97.93 % of the cumulative variances over the x-variable and y-variables blocks. As previously described, blank salt samples were represented by their ROI's average spectra, whereas for the remaining cases, where only one sample was available, randomly selected spectra from the ROI were used. Table 2 summarises the number of samples and spectra used in the model training and validation phases.

A decision threshold of 0.5 was established to discriminate between the two classes. The classification results for both training and validation sets are displayed in Fig. 4. In all cases, that is, in the 1000 iterations, classification metrics (sensitivity, specificity, and precision) reached the value of 1. For further details the confusion matrix corresponding to the external validation results is presented in supplementary material (see

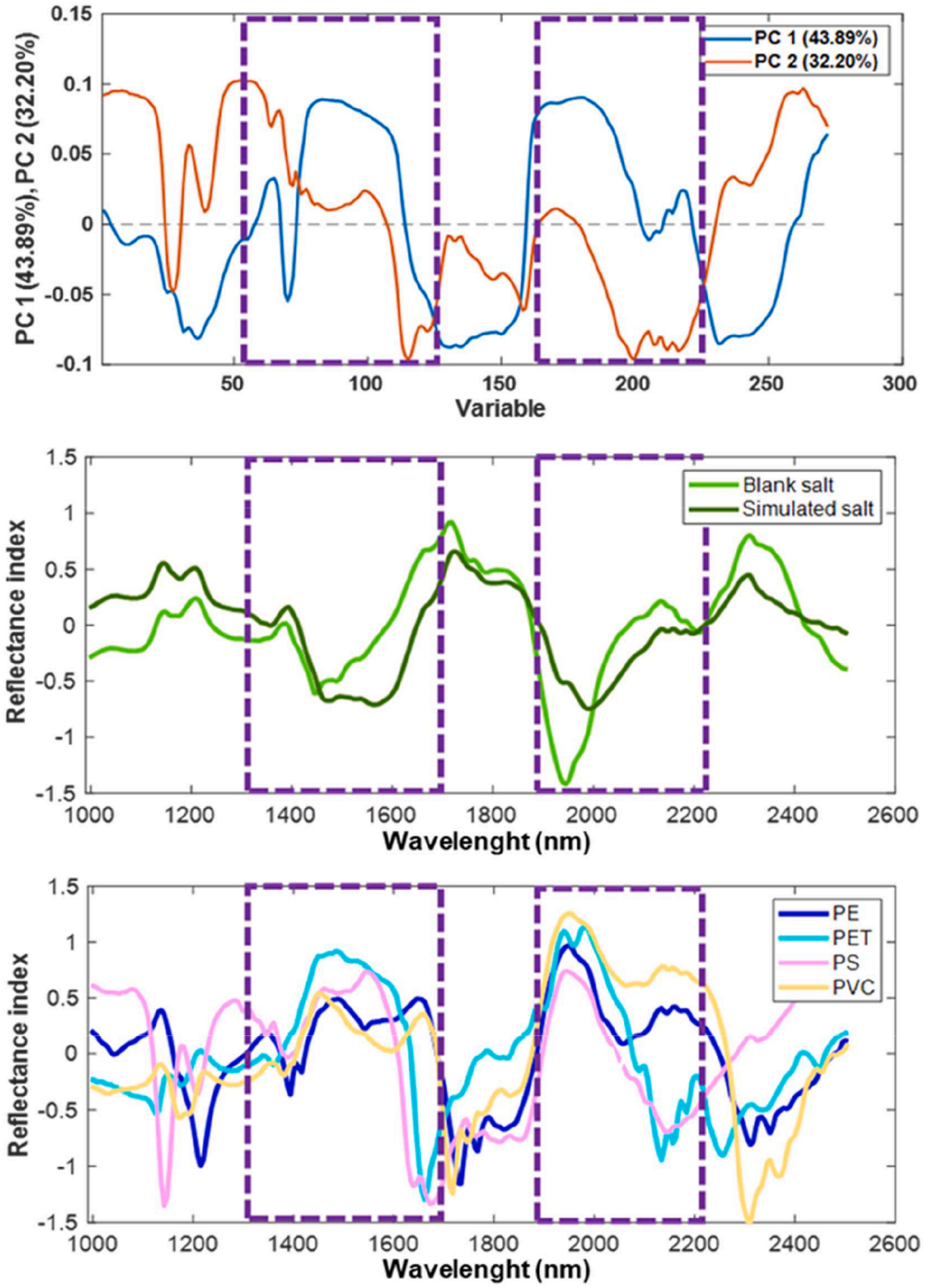

Fig. 3. Discriminating regions concerning the natural grouping of MPs-free salt and MPs samples, located over the loadings plot and the corresponding average spectra of each type of sample (MPs-free salt, PE, PET, PS, PVC).

figure S2), which shows all spectra were correctly assigned to their respective classes. These results therefore highlight the capability of the model to discriminate between MPs-free salt and MPs spectra.

3.4. Classification of PE, PET, PS and PVC

PLS-DA multiclass model was developed using randomly selected spectra from the ROI of each polymer sample. Four input classes (4iC) were defined: labelled as 'PE', 'PET', 'PS' and 'PVC' (see Table 2). The model was built selecting 3 LVs, which explained 96.12 % and 93.29 % of the cumulative variances over the x-variable and y-variables blocks. A decision threshold of 0.5 was established to discriminate between the classes.

Similarly to binary model, multiclass model performance was assessed during training, cross-validation and external validation stages. Across all evaluation stages, the sensitivity, specificity and precision classification quality metrics were calculated. All of them reached a value of 1, indicating perfect classification performance.

Fig. 5 displays the classification outcomes for each polymer class in both training and validation stages. As in binary mode, confusion matrix derived from external validation can be found in the supplementary material (see figure S3). In it can be observed, the model correctly classified every spectrum into its respective polymer class, with no misclassifications across any category.

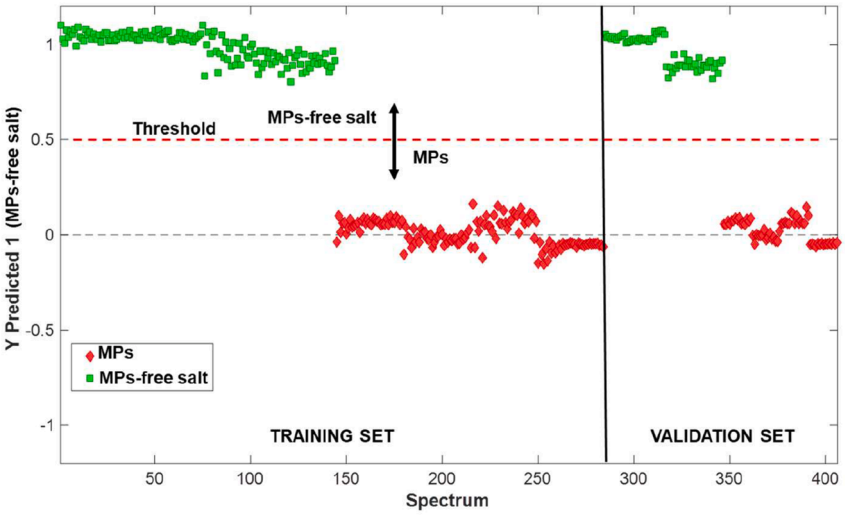

Fig. 4. PLS-DA classification results for binary model (MPs vs MPs-free salt) using both training and external validation datasets. The red line represents the 0.5 decision threshold.

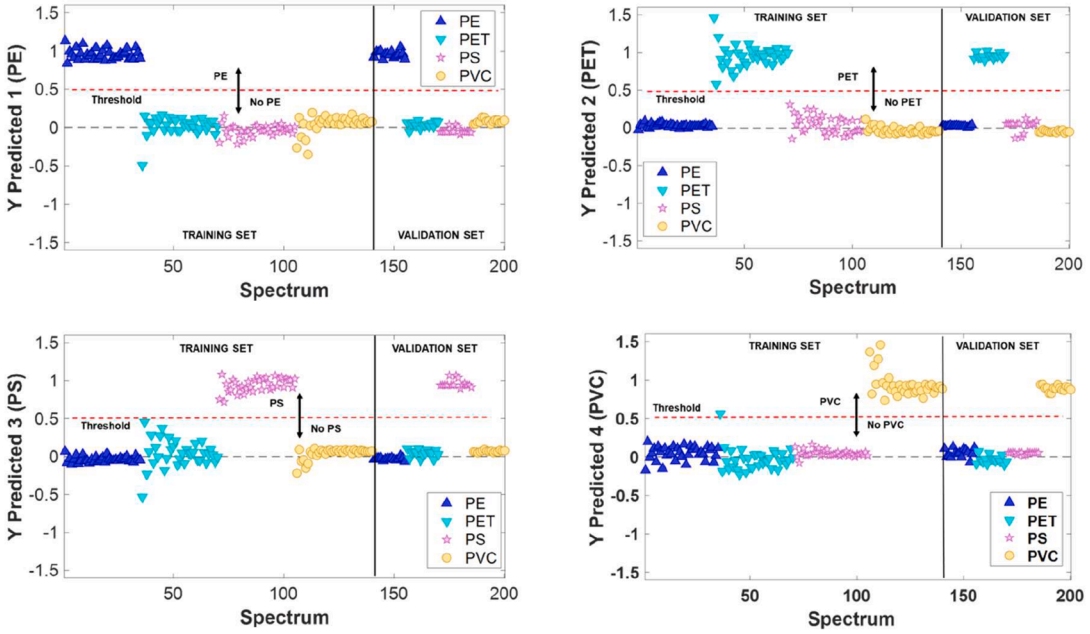

Fig. 5. PLS-DA classification results for multiclass model (PE vs PET vs PS vs PVC) applied to both training and external validation datasets. The red line represents the 0.5 decision threshold.

Table 4
Hierarchical classification results for coastal and grocery sea salt samples, including percentage of pixels classified in each class. *Note: Percentages for each polymer are expressed relative to the total number of pixels classified as MPs.*

Sea salt		% Predicted Binary model		% Predicted Multiclass model			
		MPs-free salt	MPs	PE	PET	PS	PVC
Coastal	SGC-015	99.99	0.01	14.58	85.42	0.00	0.00
	SGC-020	97.45	2.55	23.04	76.90	0.00	0.06
	SGC-029	99.82	0.18	24.49	27.51	0.00	0.00
Grocery	SME-005	99.95	0.05	6.41	80.77	0.00	12.82
	SME-006	99.99	0.01	0.00	100.00	0.00	0.00

3.5. *Detection and typification of microplastics in coastal and grocery sea salts*

Once binary and multiclass models had been trained, validated and their performance metrics assessed, attention was focused on monitoring MPs pollution in the Mediterranean Sea. For this purpose, 54 sea salts sampled from saltworks located on the Andalusian Mediterranean coast were analysed one by one.

Each sample's ROI, which comprises 331,000 spectra, was processed through the hierarchical modelling approach: binary model to determine the presence of MPs and multiclass model to assign polymer type. Out of all the samples analysed, 3 revealed evidence of MPs pollution, with proportions of MPs-classified pixels ranging from 0.01 % to 2.5 % (Table 4). Although a value of 0.01 % may appear negligible, it still represents approximately 3310 pixels identified as MPs. The most frequently detected polymers were PE and PET, with PET representing

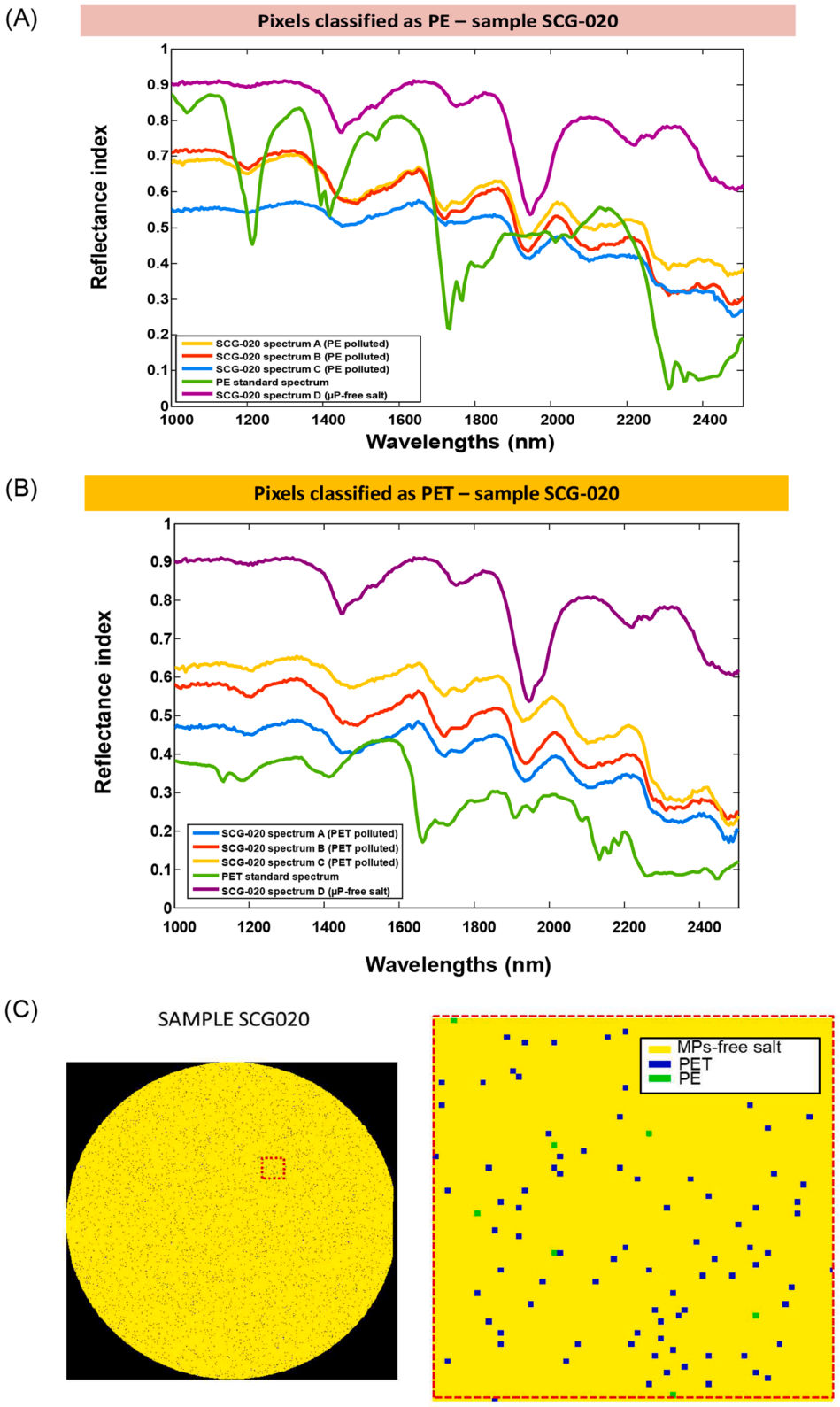

Fig. 6. Representative spectra and spatial distribution of pixels classified as MPs in coastal sea salt sample (SGC-020). (A) Random selected spectra classified as PE plotted against PE standard spectrum and spectra classified as MPs-free salt. (B) Random selected spectra classified as PET plotted against PET standard spectrum and spectra classified as MPs-free salt. (C) Colormap of the SCG-0.020 sample showing the spatial distribution of the model classification results: yellow pixels correspond to MPs-free salt, green to PE and blue to PET.

the dominant fraction in all positive cases. PVC was observed in only one polluted sample.

Additionally, six samples of grocery sea salts were analysed to assess the occurrence of MPs in commonly consumed products, which may represent a potential route of human exposure. Two of these samples were identified as polluted, with the proportion of pixels classified as MPs ranging from 0.01 % to 0.5 %. Among the detected polymers, PET was identified in both positive samples. PE and PVC were detected in one of the two polluted samples, although with relatively less abundance than PET (see Table 4).

These findings should also be interpreted considering the spatial resolution of the imaging systems. The hyperspectral camera employed in this study provided a spatial sampling resolution of 43 μm × 190 μm per pixel, meaning that each pixel corresponded to this physical area on the sample, which reaches the order of magnitude of the MPs particles. However, depending on the particle size and orientation within the field of view, the signal recorded by a given pixel may not exclusively represent the MP particle but could also include contributions from the surrounding salt matrix. Consequently, cases may occur where the particle is smaller than the pixel or positioned in such a way that the predominant contribution within that pixel arises from salt, thereby influencing the obtained spectral signal.

To further support the classification results, a subset of randomly selected pixels classified as a type of polymer from a polluted sample was examined. These spectra were displayed together with their corresponding polymer standard (i.e., PE standard spectrum if the polymer identified was PE) and a representative spectrum of the sample classified as MPs-free salt. This comparison provided an additional level of verification, as it allowed for a visual assessment of the spectral similarity of the classified pixels to their reference polymers.

As an illustrative example, a polluted coastal sea salt, particularly the sample coded as SCG-020, was selected and showed in the Fig. 6 (the remaining images showing the prediction results for polluted samples are provided in the supplementary material, Figure S4). Fig. 6A displays the spectra of pixels classified as PE, while Fig. 6B shows those classified as PET. For PE, certain characteristic peaks of the polymer standard were still visually noticeable in the spectra classified as PE, particularly around 1400–1600 nm and in the interval 1700–1800 nm. Similarly, in the case of PET, the overall spectral fingerprint of the classified pixels closely resembled that of the PET standard. It is worth highlighting that, as expected, contributions from salt spectra are present, which explains why the classified signals do not exactly reproduce those of the polymer standards.

Fig. 6C presents a colormap representing the surface of the SCG-020 sample inside the Petri dish during analysis. In this image, pixel classified as MP-free salt are coloured yellow, those identified as PE green and those corresponding to PET blue. allows a clear visualisation of MPs distribution across the polluted sample surface. For clarity, the pixels are displayed as square in the image; in reality, each pixel covers a rectangular area on the sample due to the line-scan acquisition geometry. This adjustment is purely for visualization and does not affect the spectral data or the classification results.

Importantly, in both cases, spectra from pixels classified as 'MPs-free salt' within the same sample display a markedly different spectral behaviour, confirming that the model is able to distinguish MPs from the salt matrix even when both coexist in a real environmental sample. As expected, some contribution of the salt matrix is still present in the spectra classified as MPs and conversely, which explains the deviations from the pure polymer standards and reflects realistic analytical conditions. In addition, Figure S5 (supplementary material) shows a representative area of the same sample where the classification probability of surrounding pixels is depicted, illustrating that, despite the presence of MPs embedded in a real environmental sea salt sample, the model consistently assigns high probabilities to pixels classified as MPs-free salt or MPs, further supporting the suitability of the developed strategy under realistic conditions.

4. Conclusions

This study demonstrates that NIR-HSI, when coupled with chemometrics, can be a robust, non-destructive, and solvent-free alternative to conventional analytical techniques, providing high-throughput analysis aligned with green analytical chemistry principles. Unlike traditional methods, which often require chemical reagents and extensive sample preparation, this workflow is solvent-free, does not generate chemical waste and allows direct analysis of real environmental samples. This highlights its suitability as a greener and more sustainable approach for MPs monitoring.

The proposed hierarchical classification strategy, based on two sequential PLS-DA models, proved highly effective for both discrimination between MPs and salt matrices and for typifying the polymeric nature of detected particles. The two-level model achieved perfect sensitivity, specificity, and precision in both internal and external validations, confirming its reliability and robustness. Importantly, the methodology was validated using real environmental samples of sea salts from Mediterranean saltworks and commercial products, successfully detecting and identifying MPs contamination dominated by PET and PE polymers.

By employing NIR-HSI, spatially resolved chemical information was obtained, overcoming the limitations of single-point spectroscopic approaches and enabling a representative characterization of heterogeneous samples. The imaging capability ensured that the analysis captured both the bulk composition and the localised distribution of MPs across the salt matrix.

Beyond sea salt analysis, the developed workflow provides a transferable basis for future applications in other complex environmental matrices such as sediments, soils, and food products, supporting large-scale environmental surveillance and risk-assessment initiatives within the framework of sustainable analytical chemistry.

Funding

Grant PCM_00042, funded by Conserjeria de Universidad, Investigación e Innovación and Gobierno de España and Unión Europea - NextGenerationEU.

CRediT authorship contribution statement

Miriam Medina-García: Writing – original draft, Visualization, Software, Investigation, Formal analysis, Conceptualization. **Jose Manuel Amigo:** Writing – review & editing, Visualization, Validation, Software, Methodology, Investigation, Formal analysis, Conceptualization. **Giulia Gorla:** Writing – original draft, Validation, Conceptualization. **Enmanuel Cruz-Muñoz:** Writing – original draft, Software, Conceptualization. **Davide Ballabio:** Writing – review & editing, Validation, Supervision, Methodology, Investigation. **Miguel A. Martínez-Domingo:** Writing – review & editing, Validation, Formal analysis. **Eva M. Valero:** Writing – review & editing, Validation, Formal analysis. **Ana M. Jiménez-Carvelo:** Writing – review & editing, Supervision, Resources, Project administration, Methodology, Investigation, Funding acquisition, Data curation.

Declaration of competing interest

The authors declare that they have no known competing financial interests or personal relationships that could have appeared to influence the work reported in this paper.

Acknowledgements

AMJC acknowledges the Grant (RYC2021-031993-I) funded by MICIU/AEI/501100011033 and “European Union NextGeneration EU/PRTR”. MMG acknowledges PRIORITY Cost Action (CA-20101) for the

Short-Term Scientific Mission (STSM) grant awarded for a research stay at the University of Milano-Bicocca. In addition, authors acknowledge to Salins Ibérica S.L for supplying sea salt samples from the sea coastal saltworks located in Cabo de Gata (Almeria), and to Salinas de La Malahá S.L (Granada) for supplying salt samples from the inland saltworks.

Supplementary materials

Supplementary material associated with this article can be found, in the online version, at doi:10.1016/j.greeac.2026.100327.

Data availability

Data will be made available on request.

References

[1] United Nations Environment Programme (UNEP), Microplastics: Emerging Issues, United Nations Environment Programme, Nairobi, 2016. Aviable at: chrome-extension://efaidnbmnnnibpcajpcglclefindmkaj/, https://www.nccoast.org/wp-content/uploads/2021/07/UNEP-Microplastics.pdf. accessed 9 September 2025.
[2] A. Thacharodi, R. Meenatchi, S. Hassan, N. Hussain, M.A. Arockiaraj, A. Pugazhendhi, Microplastics in the environment: a critical overview on its fate, toxicity, implications, management, and boremediation strategies, J. Environ. Manag. 349 (2024) 119433, https://doi.org/10.1016/j.jenvman.2023.119433.
[3] C.O. Okoye, C.I. Addey, O. Oderinde, J.O. Okoro, J.Y. Uwamungu, C.K. Ikechukwu, E.C. Odii, Toxic chemicals and persistent organic pollutants associated with micro- and nanoplastics pollution, Chem. Eng. J. Adv. 11 (2022) 100310, https://doi.org/10.1016/j.ceja.2022.100310.
[4] European Food Safety Authority (EFSA), Update on EFSA's activities on emerging risks 2012–2013, Parma (2014), https://doi.org/10.2903/sp.efsa.2014.EN-585.
[5] I.M. Jaikumar, M. Tomson, A. Meyyazhagan, B. Balamuralikrishnan, R. Baskaran, M. Pappuswamy, H. Kamyab, E. Khalili, M. Farajnezhad, A comprehensive review of microplastic pollution in freshwater and marine environments, Green Anal. Chem. 12 (2025) 100202, https://doi.org/10.1016/j.greeac.2024.100202.
[6] J. Aramendia, N. García-Velasco, J.M. Amigo, U. Izagirre, A. Seifert, M. Soto, K. Castro, Evidence of internalized microplastics in mussel tissues detected by volumetric Raman imaging, Sci. Total Environ. 914 (2024) 169960, https://doi.org/10.1016/j.scitotenv.2024.169960.
[7] H.A. Leslie, M.J. Van Velzen, S.H. Brandsma, A.D. Vethaak, J.J. Garcia-Vallejo, M. H. Lamoree, Discovery and quantification of plastic particle pollution in human blood, Environ. Int. 163 (2022) 107199, https://doi.org/10.1016/j.envint.2022.107199.
[8] S. Özsoy, S. Gündogdu, S. Sezigen, E. Tasalp, D.A. Ikiz, A.E. Kideys, Presence of microplastics in human stomach, Forensic Sci. Int. 364 (2024) 112246, https://doi.org/10.1016/j.forsciint.2024.112246.
[9] A. Baroni, C. Moulton, M. Cristina, L. Sansone, M. Belli, E. Tasciotty, Nano- and microplastics in the brain: an emerging threat to neural heath, Nanomaterials 15 (2025) 1361, https://doi.org/10.3390/nano15171361.
[10] C.O. Okoye, C.I. Addey, O. Oderinde, J.O. Okoro, J.Y. Uwamungu, C.K. Ikechukwu, E.C. Odii, Toxic chemicals and persistent organing pollutants associated with micro-and nanoplastics pollution, Chem. Eng. J. Adv. 11 (2022) 100310, https://doi.org/10.1016/j.ceja.2022.100310.
[11] L. Tang, J.C. Feng, C. Li, J. Liang, S. Zhang, Z. Yang, Global occurrence, drivers, and environmental risks of microplastics in marine environments, J. Environ. Manag. 329 (2023) 116961, https://doi.org/10.1016/j.jenvman.2023.116961.
[12] B. Singh, A. Kumar, Advances in microplastics detection: a comprehensive review of methodologies an their effectiveness, Trends in Anal. Chem. 170 (2024) 117440, https://doi.org/10.1016/j.trac.2023.117440.
[13] G. Chen, Z. Fu, H. Yang, J. Wang, An overview of analytical methods for detecting microplastics in the atmosphere, Trends Anal. Chem. 130 (2020) 115981, https://doi.org/10.1016/j.trac.2020.115981.
[14] G. Alak, A. Ucar, V. Parlak, M. Atamanalp, Identification, chacterisation of microplastic and their effects on awuatic organisms, Toxicol. Environ. Chem. 140 (2022) 967–987, https://doi.org/10.1080/02757540.2022.2126461.
[15] J.S. Kim, H.J. Lee, S.K. Kim, H.J. Kim, Global pattern of microplastics (MPs) in commercial food-grade salts: sea salt as an indicator of seawater MP pollution, Environ. Sci. Technol. 52 (2018) 12819–12828, https://doi.org/10.1021/acs.est.8b04180.
[16] M.P. Belioka, D.S. Achilias, Microplastic pollution and monitoring in seawater and harbor environments: a meta-analysis and review, Sustainability 15 (2023) 9079, https://doi.org/10.3390/su15119079.
[17] W.J. Shim, S.H. Hong, S.E. Eo, Identification methods in microplastic analysis: a review, Anal. Methods 9 (2017) 1384–1391, https://doi.org/10.1039/C6AY02558G.
[18] C. Vidal, C. Pasquini, A comprehensive and fast microplastics identification based on near-infrared hyperspectral imaging (HSI-NIR) and chemometrics, Environ. Pollut. 285 (2021) 117251, https://doi.org/10.1016/j.envpol.2021.117251.
[19] R. Goyetche, L. Kortazar, J.M. Amigo, Issues with the detection and classification of microplastics in marine sediments with chemical imaging and machine learning, TrAC Trends Anal. Chem. 166 (2023) 117221, https://doi.org/10.1016/j.trac.2023.117221.
[20] H. Jin, F. Kong, X. Li, J. Shen, Artificial intelligence in microplastic detection and pollution control, Environ. Res. 262 (2024) 119812, https://doi.org/10.1016/j.envres.2024.119812.
[21] M. Nyakuchena, C. Juntunen, Y. Sung, Deep-learning-assisted near-infrared hyperspectral imaging for microplastic classification, Powder Technol. 457 (2025) 120933, https://doi.org/10.1016/j.powtec.2025.120933.
[22] R. Palmieri, S. Serranti, G. Capobianco, A. Cózar, E. Martí, G. Bonifazi, Marine microplastic classification by hyperspectral imaging: case Studies from the Mediterranean Sea, the Strait of Gibraltar, the Western Atlantic Ocean and the Bay of Biscay, Appl. Sci. 14 (20) (2024) 9310, https://doi.org/10.3390/app14209310.
[23] M. Medina–García, M.A. Martínez-Domingo, E.M. Valero, L. Cuadros-Rodríguez, A. M. Jiménez–Carvelo, Detection of microplastics in sea salt using hyperspectral imaging and machine learning methods: pollution control in the Mediterranean sea as a case study, Spectrochim. Acta A Mol. Biomol. Spectrosc. 343 (2025) 126528, https://doi.org/10.1016/j.saa.2025.126528.
[24] M. Llorca, D. Álvarez Muñoz, M. Ábalos, S. Rodríguez Mozaz, L.H. Santos, V. M. León, M. Farré, Microplastics in Mediterranean coastal area: toxicity and impact for the environment and human health, Trends Environ. Anal. 27 (2020) e00090, https://doi.org/10.1016/j.teac.2020.e00090.
[25] M. Mancuso, N. Porcino, J. Blasco, T. Romero, S. Savoca, N. Spanò, T. Bottari, Microplastics in the Mediterranean Seawater, in: M. Mancuso, N. Porcino, J. Blasco, T. Romero, S. Savoca, N. Spanò, T. Bottari (Eds.), Microplastics in Mediterranean Sea, Springer, Cham, 2023, pp. 67–81, https://doi.org/10.1007/978-3-031-30481-1_3.
[26] Y. Zhang, H. Wu, L. Xu, H. Liu, L. An, Promising indicators for monitoring microplastic pollution, Mar. Pollut. Bull. 182 (2022) 113952, https://doi.org/10.1016/j.marpolbul.2022.113952.
[27] Y.S. Oren, P.M. Biesheuvel, Theory of ion and water transport in reverse-osmosis membranes, Phys. Rev. Appl. 9 (2018) 024034, https://doi.org/10.1103/PhysRevApplied.9.024034.
[28] A. Arroyo-Cerezo, A.M. Jiménez-Carvelo, M. Medina-García, E.A. Roca-Nasser, L. Cuadros-Rodríguez, Rediscovering similarity analysis of analytical signal: a not well-known mainstay of chemometrics, Trends Anal. Chem. 185 (2025) 118166, https://doi.org/10.1016/j.trac.2025.118166.
[29] L. Cuadros-Rodríguez, A. Arroyo-Cerezo, A.M. Jiménez-Carvelo, Revamping information entropy: a tailored metric for pre-evaluating quality of 2D analytical signal–A tutorial, Anal. Chim. Acta 1344 (2025) 343693, https://doi.org/10.1016/j.aca.2025.343693.
[30] M. Barker, W.S. Rayens, Partial least squares for discrimination, J. Chemom. 17 (2003) 166–173, https://doi.org/10.1002/cem.785.
[31] N.F. Pérez, J. Ferré, R. Boqué, Calculation of the reliability of classification in discriminant partial least-squares binary classification, Chemom. Intell. Lab. Syst. 95 (2013) 122–128, https://doi.org/10.1016/j.chemolab.2008.09.005.
[32] R.W. Kennard, L.A. Stone, Computer aided design of experiments, Tehcnometrics 11 (1969) 137–148, https://doi.org/10.2307/1266770.
[33] D. Ballabio, V. Consonni, Classification tools in chemistry. Part 1: linear models. PLS-DA, Anal. Methods 5 (2013) 3790–3798, https://doi.org/10.1039/C3AY40582F.
[34] L. Marchi, I. Krylov, R.T. Roginski, B. Wise, F. Di Donato, S. Nieto-Ortega, et al., Automatic hierarchical model builder, J. Chemom. 13 (2022) e3455, https://doi.org/10.1002/cem.3455.